



**INAOE**

# **Partial Volume Segmentation in Magnetic Resonance Imaging (MRI)**

**Jonás Grande-Barreto, María del Pilar  
Gómez-Gil**

**Technical Report No. CCC-17-007  
December 2017**

**Department of Computational Sciences  
National Institute for Astrophysics Optics and  
Electronics  
Tonantzintla, Puebla**

**©INAOE 2017**  
All rights reserved

The author hereby grants to INAOE permission to reproduce and to distribute  
copies of this Ph.D. research proposal in whole or in part



**Abstract:** *Image segmentation has become one of the most important tasks in medical image analysis, usually being required as the initial step for other tasks. During brain Magnetic Resonance Imaging (MRI) analysis, image segmentation provides information for the measurement and visualization of anatomical structures of the brain. Due to the spatial resolution of medical imaging equipment and complex shape of the tissue interfaces in the brain, a single pixel/voxel in a MRI may be composed of several tissue types; this phenomenon is known as partial volume-effect (PVE) and the elements affected by it are called partial volume elements (pv-elements). Typical segmentation techniques are prone to be affected by PVE by decreasing their accuracies for measuring and visualizing brain structures. To overcome the challenges produced by PVE, image segmentation techniques must estimate the contribution of each tissue in a pv-element, or at least to estimate the total amount of each tissue present in the entire image. This kind of segmentation is referred as Partial Volume Segmentation (PVS). Standard methods for addressing brain segmentation are based on pattern recognition models, assuming that each tissue is represented by a particular non-overlapped set of features. However, due to PVE, severe overlapping cases among features may be present, which leads the model to an incorrect segmentation result. To alleviate the described situation, this research looks for a solution for the PVE problem on brain MRI. The proposed scheme, based on growing regions methods, unsupervised clustering and fuzzy systems, consists of two main components. First, a hybrid intelligent model will identify slightly or non-corrupted information, in order to impose constraints for reducing overlapping among features. In a second phase, such pre-selected information features will be clustered, in order to identify boundaries that will represent each class. Classification will be based on estimating tissue proportions in each pv-element on brain MRIs and assign those elements to a single tissue class.*

**Keywords:** Partial Volume Segmentation, Magnetic Resonance Imaging, brain image segmentation, unsupervised clustering, fuzzy sets.

# Contents

<b>1</b>	<b>Introduction</b>	<b>1</b>
<b>2</b>	<b>Main Concepts</b>	<b>2</b>
2.1	Image formation . . . . .	2
2.2	MRI fundamentals . . . . .	3
2.2.1	Some Brain Components . . . . .	4
2.3	Partial Volume Effect . . . . .	5
2.4	Partial Volume Segmentation . . . . .	7
2.5	Pattern recognition . . . . .	8
2.6	Artificial neural networks . . . . .	9
2.6.1	Self-Organizing Maps . . . . .	9
2.7	Fuzzy sets . . . . .	11
2.8	Seeded Region Growing . . . . .	12
<b>3</b>	<b>Related work</b>	<b>13</b>
3.1	Region based methods . . . . .	13
3.2	Machine learning based methods . . . . .	15
3.3	Statistical based methods . . . . .	18
3.4	Hybrid methods . . . . .	18
3.5	Metrics for evaluating partial volume segmentation results . . . . .	20
<b>4</b>	<b>Problem statement</b>	<b>20</b>
4.1	Justification and Motivation . . . . .	22
4.2	Research questions . . . . .	22
4.3	Hypothesis . . . . .	23
4.4	Aim . . . . .	23
4.5	Expected contributions . . . . .	23
<b>5</b>	<b>Methodology</b>	<b>23</b>
5.1	Experiments . . . . .	26
5.2	Work plan . . . . .	27
<b>6</b>	<b>Preliminary results</b>	<b>27</b>
6.1	Synthetic images of the brain . . . . .	27
6.2	SRG extension . . . . .	28
6.3	Discussion . . . . .	31
<b>7</b>	<b>Conclusion</b>	<b>32</b>
	<b>References</b>	<b>33</b>

## List of acronyms

**ANN:** Artificial Neural Network.

**BMU:** Best Matching Unit.

**CSF:** Cerebrospinal Fluid.

**DSC:** Dice Similarity Coefficient.

**EI:** Image Element.

**FCM:** Fuzzy C-Means.

**GM:** Gray Matter.

**MRI:** Magnetic Resonance Imaging.

**pv-element:** partial volume-element.

**PVE:** Partial Volume-Effect.

**PVS:** Partial Volume Segmentation.

**ROI:** Region Of Interest.

**SOM:** Self-Organized Map.

**SRG:** Seeded Region Growing.

**TFE:** Tissue Fraction Effect.

**WM:** White Matter.

# 1 Introduction

Magnetic resonance imaging (MRI) is a noninvasive medical imaging technique that produces images from inside of the human body [Jansi and Subashini, 2014]. Commonly used in medical diagnosis, it is an invaluable tool in medicine [Pham et al., 2000]. Its working principle involves subjecting a patient to an electromagnetic field, to align hydrogen atoms in the same direction of the field. Subsequently, a radio-frequency wave is induced, which disturbs the atoms in such a way that they start to resonate [Buxton, 2009]. The resonance of such particles is measured by sensors, which send signals to a computer that converts them into an image called *slice*. The reconstructed image provides structural and functional information of the tissues. Given an MRI, one of the first and most important tasks for its analysis is to segment the image, with the purpose of detecting objects or regions of interest (ROI). Brain MRI segmentation is an essential task in many clinical applications because it influences the outcome of the entire study. During brain MRI analysis, image segmentation is used to analyze the structure of brain tissues and their changes, as well as to detect pathologies, such as tumors, abnormalities and injuries [Despotović et al., 2015]. Some of the main tissue classes of interest for brain MRI are cerebrospinal fluid, gray matter, and white matter [Jansi and Subashini, 2014].

A phenomenon that most affects a segmentation process is known as *Partial Volume Effect (PVE)*. Soret [Soret et al., 2007] describes two types of PVE, one produced by finite spatial resolution and other produced by the spatial sampling of the imaging system. This second problem is known as *Tissue Fraction Effect (TFE)*, meaning that the pixels do not fit the objects correctly. PVE causes a digital image to be blurred because there are elements whose gray value is the result of a mixture of different signals [Gruppen and Buvat, 2011]. Due to its composition, mixed elements have properties that relate to more than one ROI. The usage of inadequate approaches to deal with mixed elements in the process of segmentation may produce erroneous outputs. Artifacts found in MRI such as noise and PVE, as well as overlaps of intensities found in brain and non-brain tissues, make it difficult to find a reliable identification of tissue regions [Shattuck et al., 2001]. This way, the approach that addresses the image segmentation problem when mixed elements are considered is referred to as *Partial Volume Segmentation (PVS)* [Li et al., 2003]. PVS resides on the estimation of the contribution that ROIs have on mixed elements.

In order to overcome the PVE in the particular case of brain MRI, a number of solutions have been proposed, including methods based on intensity, statistics and machine learning [Despotović et al., 2015]. Nevertheless, those methods do not work properly for all types of brain MRI due to intensity variations, ill-defined boundaries, available information, redundant features, initial parameters, etc. In computational terms, this is still an open problem, mainly because it is ill-posed, as defined by Hadamard and commented by Marroquin [Marroquin et al., 1987]. Hybrid models are emerging approaches to deal with PVE; these models combine the strengths of two or more approaches to achieve segmentation with

improved results. However, it is required to be careful when combining approaches, because a wrong choice may lead to sophisticated structures and high computational costs.

## 2 Main Concepts

### 2.1 Image formation

Image formation takes place in a physical process where light (photons) interact with matter, and the radiation produced by this interaction is sensed by a photosensitive device (e.g. sensor or eye). Reflection, transmission and absorption are the phenomena that take place when light interacts with matter, and reflectance, transmittance and absorptance are quantities measured to describe these phenomena [Fairchild, 2013]. These measures are recorded by a sensor, quantified and finally rendered to construct a digital image. A digital image is represented by elements called pixels in the case of 2D images and voxels for 3D images (Figure 1). In this document, we used the term image element (IE) to refer to both of them. Such IEs have size, shape and spatial location. Its coordinates are commonly referred as  $(i, j)$  for pixels and  $(i, j, k)$  for voxels, where  $i$  is the image row number,  $j$  is the image column number, and  $k$  is the slice number in a volumetric stack. Furthermore, each IE has a code, which represents the intensity of the physical measure. Intensity values usually represent the code, frequently corresponding to a gray value in  $\{0, \dots, 255\}$ . The size of the element determines the spatial resolution [Lalwani and Ansari, 2012]; restricting the minimum object size that can be detected. This is important because it can help distinguish, with greater detail, features from an object. However, if the resolution size is high, the time required to process the image may be long.

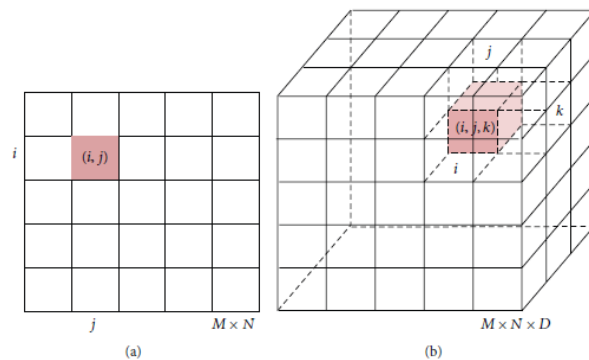


**Figure 1. Image elements in 2D and 3D space (a) For 2D space images, elements (pixels) are represented by lattice nodes, depicted as a square and (b) In 3D images, elements (voxels) are represented with lattice nodes depicted as a cube [Despotović et al., 2015]**

## 2.2 MRI fundamentals

Matter is made of atoms, where their nucleus is composed of protons and neutrons, and surrounded by an electron cloud. At equilibrium state, the number of electrons is equal to the number of protons. MRI is based on electromagnetic effects in the nucleus of the atom. In the case of the human body, which is composed of about 70% of water, MRI measures the behavior of hydrogen atoms; this is because a hydrogen atom consists of just one proton. Furthermore, the particles are in constant movement. This way, for the hydrogen atom, its movement is a self-rotation (spin, Figure 2), which has a magnetic moment [Deserno, 2011].

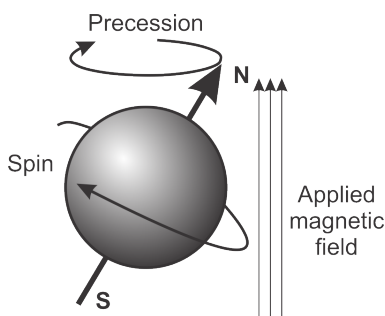


**Figure 2. Precession. A spinning proton in a magnetic field.**

The above description must be translated from particles to tissues where the spins sum up to a macroscopic magnetic moment  $M$ . Suppose an external magnetic field  $B_z$  that is oriented along the z-axis, where the magnetic moments can align parallel or anti-parallel. The following component of MRI is a Radio Frequency (RF) impulse [Deserno, 2011]; this impulse pushes the proton down with a frequency equal to the rotation rate of the proton (always at the same point of the movement) making it turn horizontally and parallel to the ground. After RF excitement, an exponential relaxation, the proton restores to its equilibrium state [Nordenskjöld, 2014]. The stored energy is released as a signal, which can be detected and transformed into an image. Two independent effects control the relaxation process:

1. T2 relaxation (*spin-spin*).- it affects the phase of the spins. For water-based and fat-based tissues, T2 is in the 40-200ms and 10-100ms range, respectively.
2. T1 relaxation (*spin-lattice*).- it affects the parallel vs antiparallel alignment of spins. For water-based and fat-based tissues, T1 is in the 400-1200ms and 100-150s range, respectively.

The repetition time ( $T_R$ ) denotes the rate of re-applying a sequence of RF, and the echo time ( $T_E$ ) is the period between a transmission and data collection [Nordenskjöld, 2014], are set to produce differently weighted images (Figure 3).  $T_1$  weighted ( $T_1$ -w) images are obtained

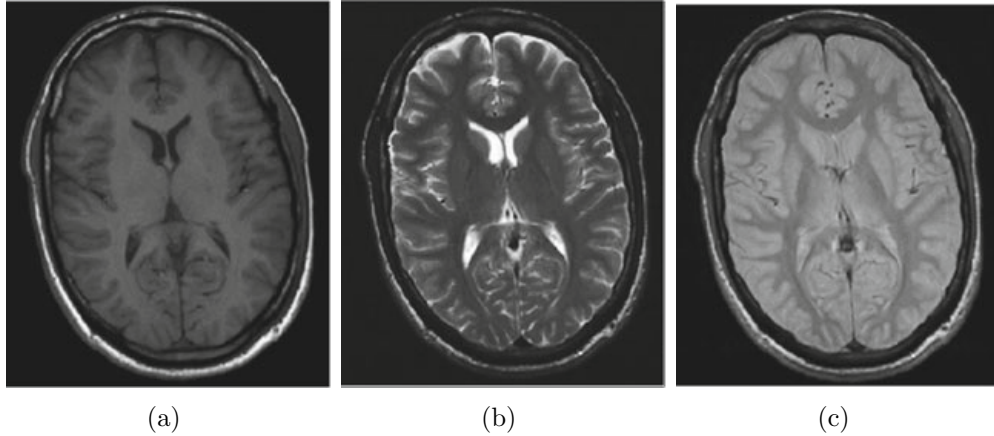


**Figure 3. Images collected using different  $T_R$  and  $T_E$  combinations. a)  $T_1$ -w, b)  $T_2$ -w and c)  $P_D$ -w [Deserno, 2011].**

if ( $T_E \leq T_2$  and  $T_R \approx T_1$ ),  $T_2$  weighted ( $T_2$ -w) images are produced if ( $T_E \approx T_2$  and  $T_R \geq T_1$ ) and proton density weighted ( $P_D$ -w) images are got if ( $T_E \leq T_2$  and  $T_R \geq T_1$ ) [Deserno, 2011].  $T_1$ -w include increased anatomic detail relative to  $T_2$ ,  $T_2$ -w is better for assessing edema and has generally shorter imaging times and  $P_D$ -w is an intermediate sequence, which seeks to combine  $T_1$  and  $T_2$  characteristics [El-Dahshan et al., 2014]. Meanwhile, on gray scale imaging, certain tissues will show up as high signal intensity, and other as low signal intensity. On  $T_1$ -w images, fluid in the tissues presents as intermediate to low signal intensity, and fat as high signal intensity. On the other hand, fluid on  $T_2$  appears as high signal and fat as low signal.

### 2.2.1 Some Brain Components

The cerebral cortex is an outer layer of different brain tissues<sup>1</sup>. The brain is protected by the skull bones of the head to prevent brain damage from outer forces. It is surrounded by cerebrospinal fluid (CSF) and by fatty tissue. The CSF has many functions, it protects the brain acting as a shock absorbent; as a medium preventing the brain from collapsing under its weight. It also works as an agent for nutrition transportation across the central nerve system [Nordenskjöld, 2014]. The cerebral cortex appears grayish brown in color and is called gray matter (GM); beneath the cerebral cortex or surface of the brain, connecting fibers between neurons form a white-colored area called the white matter (WM)<sup>2</sup>. GM surrounds the brain, but it also has some parts embedded in white matter. WM acts as a connector between regions of GM, allowing communication between different brain regions. Figure 4 depicts a simplified anatomy of the human brain seen from axial view.

<sup>1</sup><http://www.livescience.com>

<sup>2</sup><http://www.aans.org>

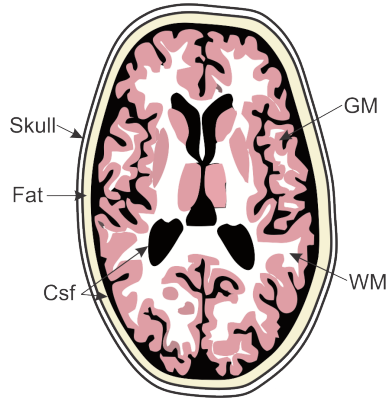


**Figure 4. Anatomy of the human brain (axial view).**

### 2.3 Partial Volume Effect

Photons are involved in many conventional imaging techniques. The difference among these techniques is the wavelength, energy level and the emission source of the imaged photons<sup>3</sup> have [Fairchild, 2013]. Photographic imaging registers the amount of reflected or emitted photons in the visible light spectrum. X-ray imaging is used to measure the number of high energy photons passing through an object. MRI uses photons to image signals coming from inside the body [Nordenskjöld, 2014]. Regardless of the image formation type that has been applied, all images may be affected by PVE. Ideally, there would be a one-to-one onto mapping from tissues to IEs gray values, which determines that the gray value of each image element represents a measure of a single tissue. Hence, grouping pixels according to their gray value could represent an object of interest almost perfectly and characterize each object according to the range of values of its level of gray [Santago and Gage, 1995]. However, due to equipment calibration, noise, physics of the tissue, quantization errors, and other factors, the gray value of an IE may be a mixture of measures from different tissues. Because of this, the range of gray values of many objects overlaps. This problem is called Partial Volume Effect (PVE), and it may refer to two different phenomena that make intensity values in images differ from what they ideally should be [Soret et al., 2007]. One possible PVE is caused by the 3D image blurring generated by a finite spatial resolution of the imaging system. As stated before, finite spatial resolution refers to the ability of the imaging system to differentiate two objects. In this case, the image is created using the convolution of the actual source with the 3D point spread function (the image of a single point object) of the imaging system (see Figure 5).

The second type of PVE is due to image sampling (see Figure 6). In this case, contours of image elements do not match the original contours of the object, which is known as TFE. Therefore, the gray value of some image elements represents the mixture of measures

---

<sup>3</sup>The amount of the detected photons by the sensors of the imaging device.

of different types of tissues. Even with the highest spatial resolution, there would still be PVE caused by image sampling [Soret et al., 2007], which occurs in the edge of structures. Furthermore, TFE is bigger if the object has large surfaces (more edge elements). In this sense, an image may contain two types of image elements:

1. *Pure elements*: they are usually the elements in the image which represent a single object.
2. *Mixed elements*: they are elements not completely occupied by a single object.

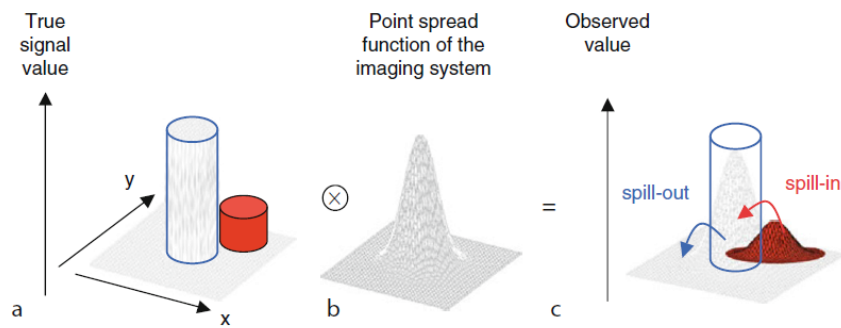


**Figure 5. PVE due to limited spatial resolution. The real signal (in a) is convoluted with the point spread function of the imaging system (in b). The result (in c) has part of the real signal spill-out (blue structure) and it is detected in the neighboring structures. Additionally, the signal coming from the neighboring structure (red structure) spill-in inside of the structure of the real signal [Gruppen and Buvat, 2011].**

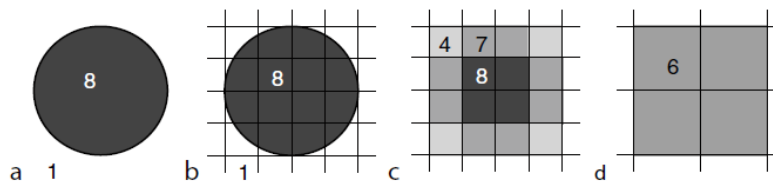


**Figure 6. PVE resulting from spatial sampling. The ROI is represented with a gray value of 8 and it is surrounded by a background with a gray values of 1 (a). Sampling with high resolution (b), taking the weighted average of the original gray values of the ROI and the underestimation is lower (c). For low resolution (d), the ROI signal intensity underestimation is larger [Gruppen and Buvat, 2011].**

## 2.4 Partial Volume Segmentation

The goal of image segmentation is to divide an image into a set of semantically meaningful, homogeneous, and non-overlapping regions of similar attributes (intensity, depth, color, or texture) [Gonzalez and Woods, 2007]. The segmentation result is a labeled image where each homogeneous region is identified [Despotović et al., 2015]. On the other hand, classification is a technique for the assignment of input patterns (image elements) to classes, based on a similarity rule. As in segmentation, classification divides elements into non-overlapping sets [El-Dahshan et al., 2014]. Segmentation and classification are related because segmentation implies the classification of each IE, and classification implies the segmentation of an image into non-overlapped classes. However, both techniques assume that every IE is a pure element, which causes problems while facing PVE. According to [Niessen et al., 1999], the misplacing of tissue borders in a 1 mm brain MR image with only a single pixel in each slice resulted in volume errors of approximately 30, 40 and 60 % for WM, GM and CSF, respectively.

Segmentation techniques incorporate tools to deal with mixed elements, known as *partial volume elements* (pv-elements) [Van Leemput et al., 2003]; for this reason, this kind of segmentation is named *Partial Volume Segmentation* [Noe and Gee, 2001, Li et al., 2003]. PVE and PVS have been addressed in various ways in MR imaging literature. The most commonly used, statistically based model of PVE is the mixel model proposed by [Choi et al., 1991]. This model assumes that each IE in an image is a pv-element whose gray value represents a weighted sum of random variables, each of which characterizes a pure tissue type. The goal in this model is to determine the relative fraction of each tissue type present within each IE. However, Choi’s model requires a significant number of parameters to estimate the necessary information to classify a single image element. Shattuck [Shattuck et al., 2001] presented a model where a new set of partial volume classes may be associated with each IE. This way, pv-elements may be separately identified using existing binary segmentation algorithms. However, an additional estimation step is necessary to obtain the fractional amount of pure tissues in each IE. Ribes [Ribes et al., 2014] presented a framework based on denoising (anisotropic diffusion) and Markov Random Fields (MRF) to address PVS on breast MR images. This work showed the importance of incorporating an efficient pre-processing stage. The main drawback of this framework is the initialization of MRF.

The above methods are based on the intensity distribution of the image. Therefore, these models are sensitive to noise. To overcome this limitation, another models had been developed; particularly those based on machine learning and combinations of two or more different methods (hybrids models) have been developed. A set of features supports most of those methods. Usually, a set of features, robust against noise and discriminative enough, supports these methods. Machine learning and hybrid methods attempt to deal with PVE as a problem of pattern recognition. Because of the lack of labeled training data, a particular interest has been developed for methods that deal with unsupervised learning.

## 2.5 Pattern recognition

Pattern recognition is formally defined as the process where a given pattern or signal is assigned to one of a prescribed number of classes [Haykin et al., 2009]. A pattern often is represented by a set of  $d$  attributes, this set of measurements is viewed as a  $d$ -dimensional array  $\mathbf{x} = (x_1, \dots, x_d)$ . The individual scalar components  $x_i$  of a pattern  $\mathbf{x}$  are called *features* [Jain et al., 1999]. Given a pattern, its recognition/classification may consist of supervised learning, in which the input pattern is identified as a member of a predefined class; unsupervised learning (clustering) in which the pattern is assigned to a class that is learned based on the similarity of patterns. A standard structure of a clustering task can be described as [Jain et al., 2000]:

1. Pattern representation.- it refers to the number of classes and number of available patterns; the number, type and scale of the features available to the clustering algorithm. This step depends on:
  - Feature extraction.- a set of transformations of the input data/features to produce new features.
  - Feature selection.- a distance function defined on pairs of patterns, in which the Euclidean distance is a common metric.
2. Pattern proximity.- it refers to a distance function defined on pairs of patterns; a common metric for evaluating pattern proximity is the Euclidean distance.
3. Clustering.- the process of grouping the input data around a prototype that represents a single class. The grouping process is based on the proximity of the patterns.
4. Data abstraction.- the process of extracting a straightforward and compact representation of a dataset. It has the purpose of improving automatic analysis (a machine can perform further processing efficiently) or it can be human-oriented (easy to comprehend and intuitively appealing); e.g. the centroid.
5. Cluster validity.- the assessment of a clustering output. The classification error or simply the error rate is the measure of the performance of a classifier. For example, the percentage of misclassified test samples is taken as an estimate of the error rate.

Jain [Jain and Dubes, 1988] formally defined partitional clustering as “*given  $n$  patterns in a  $d$ -dimensional metric space, determine a partition of the patterns into  $K$  clusters such that the patterns in a cluster are more similar to each other than to patterns in different clusters*”. Hard clustering method relates each pattern to a single cluster; where the output is a set of non-overlapped groups. A fuzzy clustering method assigns degrees of membership in several groups (each cluster is a fuzzy set of all the patterns) to each input pattern. The output of a fuzzy clustering can be transformed into a hard clustering result by assigning each pattern to the cluster with the largest membership measure; an example can be found in [Ortiz et al., 2013b].

## 2.6 Artificial neural networks

An artificial neural network (ANN) is a layered network of artificial neurons. An artificial neuron (AN) is a model of a biological neuron. Each AN receives signals from the environment, or other ANs, gather these signals, and when fired, transmits a signal to all connected ANs [Engelbrecht, 2007]. To achieve good performance, ANNs use a massively parallel number of interconnected artificial neurons [Haykin et al., 2009]. ANNs models tend to use some organizational principles (such as learning, generalization, adaptivity, fault tolerance, distributed representation and computation) in a network to learn complex nonlinear input-output relationships, use sequential training procedures, and adapt themselves to the data [Jain et al., 2000]. ANNs have been used for clustering tasks because some of the attractive features of ANNs are capable of working with numerical vectors (feature vectors), data abstraction and competitive learning [Ortiz et al., 2011, Ortiz et al., 2014]. This research makes use of ANNs to address PVS, particularly by using Self-Organizing Maps.

### 2.6.1 Self-Organizing Maps

The Self-Organizing Map (SOM) is a type of ANN composed of an input layer (input feature vectors) and one or more output layers (prototypes) [Kohonen, 2001]. Neurons are usually arranged in a two-dimensional structure, in such a way that there exist neighborhood relations among the neurons, which dictates the topology, or structure. The SOM is inspired by the neurobiological performance of the brain which is always searching for the most representative and most economical representation of data and its relationships. The goal of SOM is to transform an incoming set of feature vectors into a  $k$ -dimensional ( $k = 1, 2, 3$ ) discrete map and to perform this transformation adaptively in a topologically ordered fashion [Haykin et al., 2009]. The training algorithm for SOM is unsupervised. Training begins initializing the synaptic weights of the neurons (prototypes). This process can be done by assigning random values (between 0 and 1) to prototypes. It has been demonstrated by Kohonen [Kohonen, 2001] that “*much faster ordering and convergence follow if the initial values are selected as a regular, two-dimensional sequence of vectors taken along a hyperplane spanned by the two largest principal components of  $\mathbf{x}$* ” (i.e., principal components associated with the two highest eigenvalues). This method is called *linear initialization*. After the initialization step, three processes are followed: competition, cooperation and synaptic adaptation. These three processes are repeated until the formation of the feature map has been completed.

1. Competition.- for each input feature vector  $x$ , each neuron compares its synaptic weights  $w_j$  with the input vector. The neuron with the minimum distance is declared the winner, also called Best Matching Unit (BMU). The competition process is shown in Eq. 1:

$$i(x) = \underset{j}{\operatorname{argmin}} \|x - w_j\|, \quad j = 1, 2, \dots, l \quad (1)$$

where  $l$  is the number of neurons in the output layer.

2. Cooperation.- the winning neuron excites its neighboring neurons through a topological neighborhood function, thereby providing the basis for a the cooperation process among such neighborhood.
3. Synaptic adaptation.- the excited neurons adjust their synaptic weights according to the input feature vector with the purpose of enhancing response of the winning neuron to the subsequent application of similar input feature vectors [Haykin et al., 2009]. The synaptic adaptation of weights is given by equation

$$w_j(n+1) = w_j(n) + \eta(n)h(i(x), j)(x - w_j(n)) \quad (2)$$

where  $h(i(x), j)$  is the topological neighborhood centered on the winning neuron  $i$  and encompassing a set of excited neurons  $j$ , and provides the influence that the winner has over neighboring neurons.  $\eta$  is the learning rate parameter, it decreases gradually with increasing time  $n$ . This requirement can be satisfied by the following heuristic recommended by [Haykin et al., 2009]

$$\eta(n) = \eta_0 \exp\left(-\frac{n}{\tau}\right) \quad j = 1, 2, \dots, \quad (3)$$

where  $\tau$  is a time constant and  $\eta_0$  is the initial value of the learning rate.

Once the feature map has been completed, the quantization error  $q_e$ , which determines the average distance between each data vector and its BMU, and topological error  $t_e$ , which measures the proportion of data vectors for which first and second BMUs are not adjacent units, are used to calculated to measure the goodness of the map [Kohonen, 2001].

$$q_e = \sum_{i=1}^N \|\vec{x}_i - \vec{w}_{\vec{x}_i}\| \quad (4)$$

$$t_e = \frac{1}{N} \sum_{i=1}^N \mu(\vec{x}_i) \quad (5)$$

In Eq. 4,  $\vec{x}_i$  is the  $i$ th data vector on the input space and  $\vec{w}_{\vec{x}_i}$  is the weight (prototype) associated with the best matching unit for the data vector  $\vec{x}_i$ . In Eq. 5,  $N$  is the total number of data vectors,  $\mu(\vec{x}_i)$  is 1 if the first and the second BMU for  $\vec{x}_i$  are non-adjacent and 0 otherwise.

## 2.7 Fuzzy sets

In a crisp set, membership of element  $x$  in a set  $A$  is described by a characteristic function

$$\mu_A(x) = \begin{cases} 1 & \text{If } x \in A \\ 0 & \text{otherwise} \end{cases} \quad (6)$$

Fuzzy set theory extends this concept by defining partial membership. Zadeh [Zadeh, 1965] formally defined as “A fuzzy set  $A$  in  $U$  may be represented as a set of ordered pairs. Each pair consists of a generic element  $x$  and its grade of membership function”; that is  $A = \{x, \mu_A(x) | x \in A\}$ . Here,  $\mu_A(x)$  takes values in the interval  $[0, 1]$ . Fuzzy sets have been used for estimating the spatial extension of ROIs. Cheng [Cheng, 2002] proposed four types of representations for ROIs when ambiguity affects the boundaries among them. This kind of representations are called fuzzy objects and are described as:

- **Fuzzy-Fuzzy area.**- the object is called a *fuzzy-fuzzy object*; the first *fuzzy* means that its spatial extent is fuzzy; the second *fuzzy* implies that its interior is fuzzy because it contains elements that have been assigned to the ROI with a certainty less than 1.
- **$\alpha$ -cut.**- a threshold value  $\alpha$  is defined with the purpose of delimiting zones in a fuzzy-fuzzy area. If different  $\alpha$  are defined, each value will be called  $\alpha$ -cut boundary. These internal limits are defined to separate elements with different levels of certainty.
- **Conditional boundary.**- area ROIs are defined as being spatially disjoint in space, i.e., each element belongs in principle to a single ROI. Although the boundary between two objects cannot be located crisply, the conceptual model suggests that a particular location should either belong to only one object.
- **Core-transition zone.**- when a clear boundary cannot be defined, but there are transition zones between the ROIs. In the transition zones, no decision is made about which object might belong to.

Fuzzy sets have been used to overcome the effect of noise and PVE in medical image segmentation [Wang and Chen, 2012, Zhang et al., 2017]. Particularly, Fuzzy C-Means (FCM) has become a recurrent method for the partition of data into different groups by using fuzzy sets [Bezdek et al., 1981]. In FCM, data points may be assigned to more than one cluster depending on their membership degree to different clusters. As a result, this method can outperform crisp methods in real applications, especially when clusters are not well separated, the borders of the clusters are not sharp, and clusters overlap [Budayan et al., 2009]. FCM is based on the minimization of the following objective function

$$J_m = \sum_{i=1}^D \sum_{j=1}^N \mu_{ij}^m \|x_i - c_j\|^2, \quad 1 \leq m \leq \infty \quad (7)$$

where,  $D$  is the number of data points.  $N$  is the number of clusters,  $m$  is the fuzzy partition matrix exponent controlling the degree of fuzzy overlap, with  $m > 1$ .  $x_i$  is the  $i$ th data point.  $c_j$  is the center of the  $j$ th cluster.  $\mu_{ij}$  is the degree of membership of  $x_i$  in the  $j$ th cluster. For a given data point,  $x_i$ , the sum of the membership values for all clusters is equal to 1.

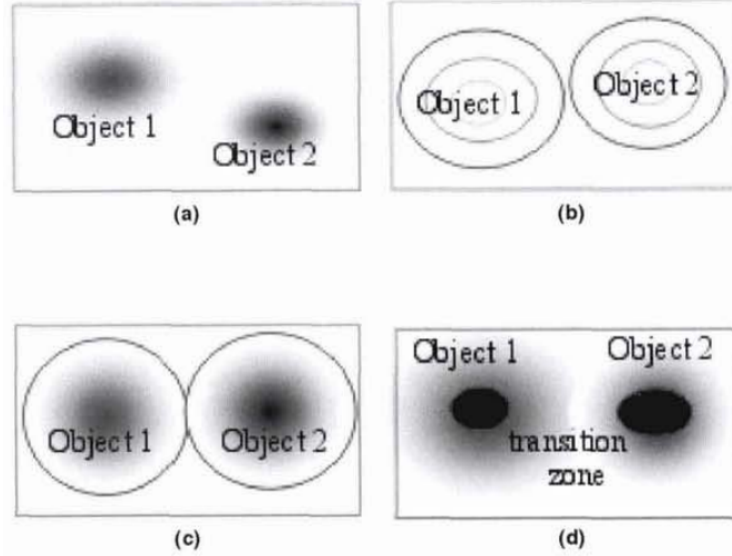


**Figure 7. Representation of fuzzy objects. (a) Fuzzy-Fuzzy area. (b)  $\alpha$ -cut. (c) Conditional boundary. (d) Core-transition zone [Cheng, 2002].**

## 2.8 Seeded Region Growing

Region growing also known as Seeded Region Growing (SRG) is a segmentation technique proposed by [Adams and Bischof, 1994] to extract large connected regions of IEs with similar features starting from initial points called *seeds*. SRG algorithm needs  $n$  seeds sets  $S = \{S_1, S_2, \dots, S_n\}$ . Seeds can be placed manually or automatically, this process is called *seeding* and plays an important roll in the performance of SRG because at least one seed must exist for each region of interest. From seeds, new elements (neighbors) are included in a particular area  $R_1, R_2, \dots, R_n$ , if they meet an homogeneity criterion  $\delta(x)$  evaluated from the gray levels of the region (statistical moments, parameters of texture, Bayesian approaches), this process is called *growing*. The IEs in the same region are labeled by the same symbol and the IEs in different regions are labeled by different symbols. These set of IEs are called the *allocated* IEs, while the others are called the *unallocated* IEs [Fan et al., 2005]. Let  $H$  be the set of all unallocated IEs that are adjacent to at least one of the labeled regions

$$H = \left\{ (x) \notin \bigcup_{i=1}^q R_i \mid N(x) \cap \bigcup_{i=1}^q R_i \neq \emptyset \right\} \quad (8)$$

where  $N(x)$  is the neighborhood of the IE. Now, if the unlabeled IE  $(x) \in H$  matches one of the labeled image region  $R_i$ , defined as  $\varphi(x) \in \{1, 2, \dots, q\}$ , such that

$$N(x, y) \cap R_{\varphi(x)} \neq \emptyset \quad (9)$$

then,  $\delta(x, R_i)$  is defined to measure how different is  $x$  from the region  $R_i$  that intersects  $N(x)$ . The simplest definition for  $\delta(x)$  proposed by [Adams and Bischof, 1994] is

$$\delta(x, R_i) = |g(x) - \text{mean}_{y \in N_i}(g(y))| \quad (10)$$

where  $g(x)$  is the gray value of the image point  $x$  and  $N_i$  is the neighborhood round point  $x$ . If  $N(x)$  meets two or more of the labeled regions,  $\varphi(x)$  takes a value of  $i$  such that  $N(x)$  meets  $R_i$  and  $\delta(x, R_i)$  is minimized.

$$\varphi(x, R_i) = \min_{x \in H} \{\delta(x, R_j) | j \in \{1, \dots, q\}\} \quad (11)$$

A seed keeps growing until there are no more unallocated IEs or a stop condition is reached. However, the main disadvantage of SRG is to be affected by spread outside the ROI since the process cannot distinguish connected structures with similar properties [Zanaty and Asaad, 2013]. Revol [Revol-Muller et al., 2013] proposed two formalisms for grouping the extensions of SRG. The first formalism is feature space oriented. It allows processing whatever kind of data (e.g. gray levels, physical parameters, spatial coordinates). Its advantage is to define a robust neighborhood, i.e., a set of points belonging to the targeted population without considering outliers. The second formalism describes SRG as an iterative and convergent process driven by an energy minimization. This formalism is used to take into account whatever kind of energy based on different types of information, e.g., contour, region or shape.

### 3 Related work

This section presents related works to PVS on brain MRI. First, single models are reviewed by discussing their approaches and limitations. Then, hybrid models are analyzed in a similar way as single models. Methods that deal with brain segmentation but do not address PVS are not the main focus of this research, therefore, they are not discussed in depth.

#### 3.1 Region based methods

Region based methods use local intensity or descriptive statistics, like mean and standard deviation, together with a minimization framework to achieve segmentation. Some examples of these methods are thresholding, region growing and watershed. Thresholding is a simple, efficient and well-known tool to separate object's ROIs. Thresholding uses a single or composed value called thresholds  $\tau$  to achieve the desired partition. In its simplest form, thresholding uses a single value proposed from histogram analysis [Gonzalez and Woods, 2007].

Thresholding can be modeled in sophisticated ways to be robust against noise and artifacts in the image [Sezgin et al., 2004]. Nevertheless, thresholding is not an appropriate solution to deal with PVS since it does not consider the existence of mixed elements. On the other hand, thresholding can be used to separate non-brain elements from brain elements [Dogdas et al., 2005, Douaud et al., 2007]. An interesting approach for dealing with PVS on bone analysis is presented in the work of Thevenot [Thevenot et al., 2014].

Lin [Lin et al., 2012] addressed tissue brain segmentation with a combination of multi-spectral MRI (see Figure 8) and fuzzy knowledge (fuzzy edge determination and fuzzy similarity computation) to improve the seed and growing process in a modified SRG. Even if the model does not address PVE directly, the usage of multi-spectral MRI and fuzzy knowledge could provide a solution. Nevertheless, due to its multi-spectral approach, the author does not provide information about the performance of the model if there are not multi-spectral data. For evaluating the performance of his model, the author uses Dice Similarity Coefficient (DSC), also known as the overlap index or  $F_1$ . Péporté [Péporté et al., 2011] proposed a hybrid approach to segment premature infant brain tissues from MRI. This model combines K-means and SRG to segment brain tissues (GM and WM), aiming at skull-stripping. According to the author, there is a weak point in the delimitation of boundaries between CSF and brain tissues, which remains an unsolved problem. The author uses the Jaccard (JAC) index to evaluate the performance of his model [Taha and Hanbury, 2015].

$$DSC = \frac{2|S_g \cap S_t|}{|S_g| \cup |S_t|} \quad (12)$$

$$JAC = \frac{|S_g \cap S_t|}{|S_g| \cup |S_t|} \quad (13)$$

where  $S_g$  and  $S_t$  are the ground truth and outcome from the model respectively.  $|\cdot|$  is the cardinality of the set. Nevertheless, due to its multi-spectral approach, the model may not work if there is not available these type of multi-spectral data. Zanaty [Zanaty and Asaad, 2013]

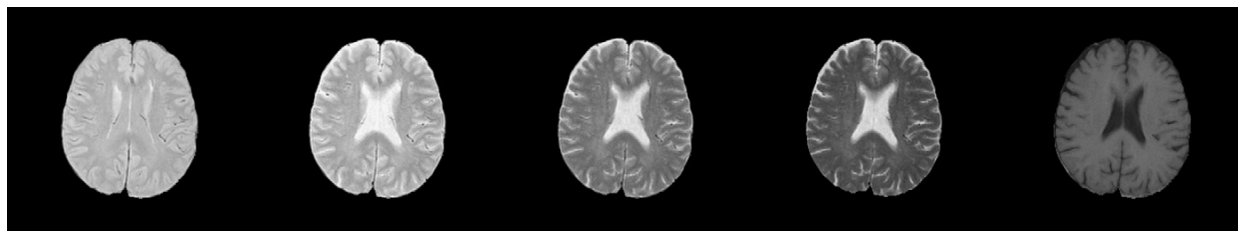


**Figure 8. Multi-channel brain MRIs acquired from different pulse sequences of TR and TE [Lin et al., 2012].**

proposed an extension of SRG which is based on a probabilistic approach for calculating a multi-threshold function for the homogeneity criterion. This function defines a threshold

value for a particular region regarding with a local neighborhood and probability of each IE of the region. The seed process is carried out by manual operation. On the other hand, the success of the method relies on the proper selection of a set of values, which are fixed manually for the whole MRI volume. Morales [Morales et al., 2014] presented an extension of SRG to separate pure IEs from pv-element in remote sensing images. The seeded process was achieved with a genetic algorithm that combines a sub-regions (obtained with watershed algorithm [Haris et al., 1998]) into homogeneous groups. Centroids for each cluster are calculated and used as a reference point to select the best seeds in the group. New IEs are added to the seeds until a stop condition is reached. Only the data distributed in the first standard deviation are designed as pure IEs of each homogeneous coverage. Because the model was designed to work with remote sensing images, there are no comments from the authors about the performance of the model with single-band images or its application to other multi-spectral domains.

### 3.2 Machine learning based methods

Machine learning based methods use features (typically features are intensity and texture) to classify the IEs and achieve a partition among ROIs. FCM is a well-known classification method because it can handle uncertainty (noise and PVE). FCM allows performing adjustments on its operating parameters that provide good results. These modifications can be divided into two groups: methods evaluating the segmentation performance by modifying the object function, and methods assess the segmentation performance by modifying the membership value [Kang and Kim, 2014]. Modifications on FCM try to include robustness against noise and spatial constraints but at the same time introduce computation issues, by changing most equations along with the change in the objective function, and have to lose the continuity from FCM [Shen et al., 2005]. However, the principal drawback for FCM is its random initialization, which provokes that the algorithm needs to be executed several times to ensure a correct result [Wang et al., 2008]. Kannan [Kannan et al., 2012] introduces an extension of FCM, called robust fuzzy c-means based kernel function (RFCMK), which replaced the original Euclidean distance with properties of kernel function on feature space. Furthermore, RFCMK includes cluster initialization. However, the RFCMK structure turns sophisticated and highly dependent on the value of  $\alpha$  and  $\beta$ , but the author does not give the guidelines or restrictions to choose them. Table 1 describes some extensions of FCM algorithm for the classification of pv-elements.

Concerning ANN, the SOM network is designed to work as an automatic unsupervised data-analysis method. The SOM has been used in image segmentation and clustering tasks [Kohonen, 2013]. The main advantage of SOM in segmentation is the use of topological information, since a set of prototypes can represent a cluster. Ortiz [Ortiz et al., 2013a] proposed two variations of SOM to identify CSF, GM and WM on brain MRI. The first method is called HFS-SOM, it aims to model peaks and valleys of the histogram as it retains discriminative information for the classification task. Initialization of SOM prototypes is performed by using the two largest principal components from the input set. Figure 9 depicts the

**Table 1. Related works for classification of brain MRI by using FCM extensions.**

Author	Relevant features	Data	Metric
[Zhang et al., 2017]	Peak detection is used to initialize cluster centers, spatial information provide robustness to artifacts and reallocation of the misclassified pixels refines segmentation result	Synthetic Real	JAC
[Gong et al., 2013]	Euclidean distance was replaced by kernel metric to incorporate local information	Synthetic Real	JAC
[Sikka et al., 2009]	Automatic cluster calculation. Several initial parameters must be manually tuned	Synthetic Real	DSC
[Liao et al., 2008]	Spatial constrained kernel and bias field correction, provide a robust and fast performance	Synthetic Real	JAC

grouping processes, the most similar prototypes have similar colors, and their size represents the number of activations of each group (prototypes with a higher number of activations have a larger size). The second method named EGS-SOM uses a feature vector composed of some first order statistics (IE’s gray value, mean, and standard deviation), 14 texture features proposed by [Haralick et al., 1973] and 7-moment invariants defined by [Hu, 1962]. EGS-SOM incorporates a feature selection process, inspired by the work of Güler [Güler et al., 2009] where feature vectors optimization were achieved by PCA, based on a Genetic Algorithm (GA). SOM prototypes are grouped by calculating the entropy gradient for each of them.

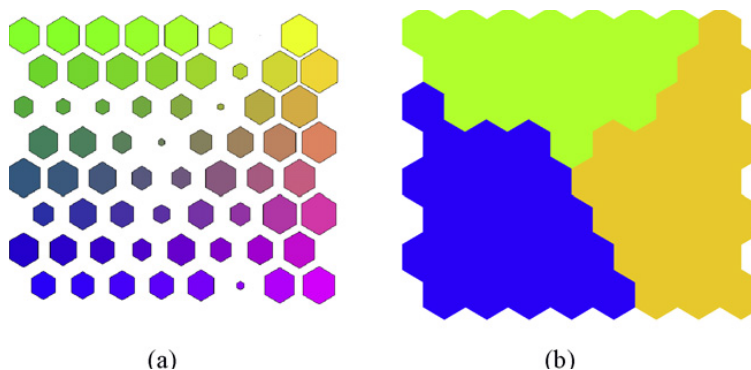


**Figure 9. Prototype activation (a) and clustering result after computing the clusters with the  $k$ -means algorithm for 3 clusters (b) [Ortiz et al., 2013a].**

About the performance of both methods, HFS-SOM is computationally efficient and allows the segmentation of the whole volume at once, insofar as images do not contain severe intensity inhomogeneities (caused by non-uniformities in the radio frequency field during acquisition). The author used the JAC index to measure the accuracy of the two methods.

HFS-SOM reports  $0.60 \pm 0.08$  of accuracy for WM and  $0.60 \pm 0.09$  for GM. On the other hand, EGS-SOM provides better results than HFS-SOM  $0.76 \pm 0.04$  for WM and  $0.73 \pm 0.05$  for GM. EGS-SOM is robust against noise and inhomogeneities because it incorporates optimized features but at considerable computational cost. SOM also is used to help other methods in their limitations, Anitha [Anitha and Murugavalli, 2016] used SOM to generate a training examples for a KNN classifier. Similarly, Abdelsamea [Abdelsamea et al., 2015] used SOM for guiding an active contour model, named Self-Organizing Active Contour (SOAC), for segmenting brain tissues. In SOAC model, it is assumed that training examples belonging to the true foreground  $\Omega^+$  and true background  $\Omega^-$  of a training image are available  $I^{tr}$ . Then, two different SOMs are trained using, respectively, the two training sets. In such a way, the neurons of each SOM self-organize to learn, respectively, the topological structures of the intensity distributions of the true foreground/background. Furthermore, the SOAC model can be extended to the case of vector-valued images. Such an extension is particularly useful for the segmentation of multi-spectral images. In the vectorial case, the image  $I(x)$  is composed by  $D$  channels  $I_i(x)$ , with  $i = 1, \dots, D$ . The limitation presented by the SOAC is the selection of training examples, manually selected, there is not a description of the size of the SOMs either of it data representation quality by the maps, and the  $r_0$ ,  $\sigma$  and  $\sigma'$  parameters must be tuned manually for each image.

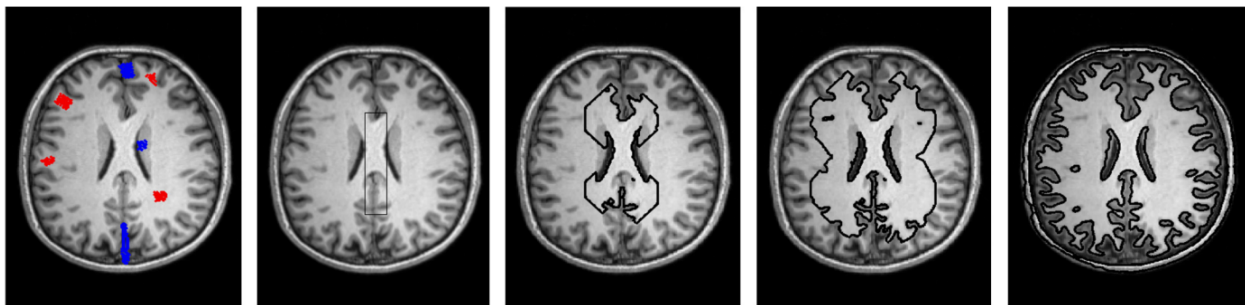


**Figure 10. Segmentation results obtained by the SOAC model on brain MRI. The training examples used by the SOAC model (in red for the foreground, in blue for the background). The initial contours (rectangle) evolves at three successive stages of SOAC [Abdelsamea et al., 2015].**

Liu [Liu et al., 2010] presented a modification in the training of SOM that allows it train in a supervised fashion way. The modification called *tagging* expands the dimension of training samples to  $N + k$ , where  $N$  is the dimension of training samples and  $k$  the number of classes. The class information is embedded into the training samples in the form of binary coding. After training, the model incorporates FCM to address pv-elements classification regarding clusters. However, a drawback of this work is that does not provide an evaluation metric of its performance because of the lack of ground truth.

### 3.3 Statistical based methods

Statistical based methods label IEs according to probability values, which are usually determined based on the intensity distribution of the image. For brain MRI segmentation, often it is assumed that the IEs intensities are independent samples from a mixture of Gaussian probability distributions [Despotović et al., 2015]. [Xia et al., 2016] proposed a model based on learning Local Variational Gaussian Mixture (LVGM) models, assuming that the intensities of the tissues classes are Gaussian distributed even though the distributions are in fact Rician. This assumption simplifies calculations, and the errors produced by it are acceptable. However, in reality, the standard deviations of some tissue types are more significant than others, so assuming that all standard deviations are equal is not realistic [Zhang et al., 2001].

On the other hand, MRF modeling itself is not a segmentation method but a statistical model that it is usually incorporated into segmentation methods. MRFs model spatial interactions among neighboring IEs. In medical imaging segmentation, they are used because most IEs belong to the same class as their neighboring IEs. This relation implies that any anatomical ROI formed by a single IE has a very low probability of occurring under MRF assumption [Pham et al., 2000]. [Ahmadvand and Daliri, 2015] used MRFs for reallocating a sub set IEs on each cluster, which have lowest belonging to their cluster. The initial partition was achieved by two approaches, FCM and a combination of Genetic Algorithm and Gaussian Mixture Models (GA-GMM). The author proposed two energy functions; the function selection depends on which method was used to achieve the initial partition. Then, MRFs are used for classifying and improving the initial segmentation. A possible limitation of this model may be that does not address CSF class, being this class which presents the most severe PVE affectation since it is present in the interfaces CSF-GM and CSF-WM

### 3.4 Hybrid methods

Appropriate selection technique for a given application is often a trade-off among robustness against noise and inhomogeneities, accuracy and computational efficiency. A combination of several techniques may be necessary to obtain the segmentation goal. This combination is called a *hybrid approach*, and it combines different complementary methods into a unified approach to overcome many of the disadvantages of each single method and achieves specific goals that others cannot reach [Despotović et al., 2015]. Table 2 describes some hybrid models. The critical issue of hybrid based segmentation methods is their *increased complexity* (time and space complexity) compared with single models. These methods also have to deal with several parameters that need to be tuned. Furthermore, it is essential that the outcome from a previous method be suitable or require the minimum post-processing for the next method. Furthermore, the combination of many individual methods may require considerable computational resources or substantial computation burden. Therefore, a hybrid segmentation method should be carefully and wisely designed to provide good quality and efficient performance.

**Table 2. Related works for hybrid classification approaches.**

Author	Segmentation technique	Relevant features	Disadvantages
[Lötjönen et al., 2010]	Multi-atlas+EM	Atlas selection is done based on an intensity-based similarity. The EM algorithm is applied for a multi-object segmentation	The major limitation is that images to be segmented and atlases used should be acquired approximately similar imaging parameters
[Liu and Guo, 2015]	K-means+SVM	K-means is used to generate training examples and initial partition. SVM uses the data from K-means to refine the initial partition	The random initialization of K-means demands several runs to secure a correct result. SVM training needs to be executed for each
[Gui et al., 2012]	MRF+ACO+GA <sup>1</sup>	The high-level knowledge guides specific segmentation functions (watershed and active contours), making the model fully automatic	It is a highly elaborated method since it has several subprocess
[Ortiz et al., 2013b]	FCM+GA <sup>2</sup> +SOM	The combination of FCM-SOM provides an efficient partial volume estimation	Feature optimization was performed mixing information of pure and mixed IEs
[Agahari and Chandrashekar, 2017]	SOM+EFCM	Feature prototypes (frequency and statistics) are input to the SOM for coarse clustering. The codebook vectors of the trained SOM are clustered automatically using EFCM.	The model has problems dealing with non-gaussian noise. Prototype clustering relies upon a manual tuning
[Sainju et al., 2014]	SRG+MLP	SRG obtains homogeneous regions from which features for classes are extracted. Then, a MLP uses these features for identifying bleeding regions	SRG require manual tuning
[Helmy and El-Taweel, 2016]	SIST+SOM+PCNN	The inverse SIST together with SOM is used for a preliminary classification. PCNN refines the SOM results to reduce the over-segmentation artifacts	The SOM and PCNN parameters need adjusting through successive iterations

EM=Expectation Maximization

GA<sup>1</sup>=Gossip Algorithm

SRG=Seeded Region Growing

PCNN=Pulse-Coupled Neural Network

SVM=Support Vector Machine

FCM=Fuzzy C-Means

EFCM=Extended Fuzzy C-Means

MRF=Markov Random Fields

GA<sup>2</sup>=Genetic Algorithm

MLP=Multilayer Perceptron

ACO=Ant Colony Optimization

SOM=Self-Organized Map

SIST=Shift-Invariant Shearlet Transform

### 3.5 Metrics for evaluating partial volume segmentation results

The evaluation of the results of a partial segmentation method depends on the application domain. In real images where ground truth does not include partial labels, the quantitative assessment is restricted to evaluate the quality of the subsequent hard segmentations. For example, [Tohka, 2013] and [Ahmadvand and Daliri, 2015] used MRF for computing an estimate of the fractional tissue content of each of the three main tissue types (WM, GM and CSF) in each IE. Then, they classify the IEs regarding with the maximum fractional tissue content. Quantitative evaluation is performed with JAC index and DICE coefficient. In similar way, [Ortiz et al., 2013b] presented a model with a soft classification approach to address the classification of pv-elements and used the maximum membership criterion to assign these elements into a single class.

On the other hand, when it is available a partial label ground truth, there are metrics for quantitative evaluation of the uncertainty. [Morales, 2014] presented a model for soft classification of pv-elements in remote sensing images. The author used a metric called Class-specific Fuzzy Certain Measure (CFCM) proposed by [Schiewe and Kinkeldey, 2009], equation (14) describes the CFCM

$$CFCM(c) = 1 - \frac{1}{n} \sum_{i=1}^n |\mu_{i,REF}(c) - \mu_{i,class}(c)| \quad (14)$$

$$\forall i | \mu_{i,REF} > 0 \cup \mu_{i,class} > 0$$

where  $\mu_{i,REF}(c)$  is the class membership value of a pixel/area for class  $c$  in reference data,  $\mu_{i,class}(c)$  is the class membership value of a pixel/area for class  $c$  in classification data and  $n$  is the number of pixels/areas under examination. The interpretation of (14) is that if a value  $\approx 1$  is obtained, it means that there is a high match for the object of the class  $c$  between the reference data set and the classification result. [Crum et al., 2006] proposed overlap measures for multiple labels namely  $JAC_{ml}$  and  $DICE_{ml}$ , equation (14) describes  $JAC_{ml}$

$$JAC_{ml} = \frac{\sum_{labels,l} \sum_{voxels,i} MIN(A_{li}, B_{li})}{\sum_{labels,l} \sum_{voxels,i} MAX(A_{li}, B_{li})} \quad (15)$$

where  $A_{li}$  is the value of voxel  $i$  for label  $l$  in segmentation  $A$  (analogously for  $B_{li}$ ) and  $\alpha$  is a label-specific weighting factor that affects how much each label contributes to the overlap accumulated over all labels. Here, the  $MIN(\cdot)$  and  $MAX(\cdot)$  are the norms used to represent the intersection and union in the fuzzy case.  $DICE_{ml}$  can be then calculated from  $JAC_{ml}$  with  $DICE_{ml} = 2JAC_{ml}/(1 + JAC_{ml})$ .

## 4 Problem statement

PVE may affect the structural information of digital images and its characterization since it modifies the structure of ROIs. Even with the existing high-resolution devices, PVE

is not reduced to a desirable level because the problem moves to other zones on the image [Christiansen, 2016]. There is a particular interest to solve the problems that PVE presents in the structural characterization of the brain analyzed from MRI. There are several methods reported in literature about brain MRI segmentation. Most of those methods address brain segmentation as a pattern recognition task where the image is transformed into a set of relevant features [Ortiz et al., 2013a, Liu and Guo, 2015, Helmy and El-Taweel, 2016]. This approach is made under the assumption that each ROI will be represented by a particular set of features.

However, images affected by PVE have severe overlapping cases among the features that represent each ROI, which leads models to an incorrect segmentation result. Even when an optimization process is applied to the selected features, it may be possible that this process fails in its purpose because the structures are severely affected by PVE [Péporté et al., 2011]. Furthermore, the lack of labeled training data demands models to be capable of learning from the data in an unsupervised manner for identifying information free or, at least, corrupted at minimum level by PVE [Anitha and Murugavalli, 2016].

An initial partition between homogeneous regions and regions formed by pv-elements may provide information (gray level distribution, spatial location and/or topological relationships) that help models to impose stronger constraints for reducing the overlapping among the features of the ROIs [Thevenot et al., 2014, Morales, 2014, Abdelsamea et al., 2015]. Furthermore, this information may be used as a training set in such way that models can learn in a supervised way when there is a shortage of training data. Therefore, we assume that this approach may improve the classification of pv-elements in structural characterization of brain tissues.

The problem to be addressed in this research is focused on detecting and separating homogeneous regions from T1-weighted scans of the brain, such that the information of these areas can be used for estimating the tissue proportions in pv-elements. We selected T1-weighted scans because they provide the best scan resolution, and are useful for localizing anatomical structures unlike with T2-weighted which is helpful for detecting pathologies [Deserno, 2011, Li et al., 2015]. The proposed solution consists of a hybrid model that identifies and selects reference information (points/regions) that represent the CSF, GM and WM classes. This information will be obtained from:

- Gray distribution and spatial location.- an extension of the SRG algorithm will be implemented with the purpose of identifying the location and gray level of IEs affected at a minimum level by PVE. Subsequently, each IEs will be represented by a feature vector composed of gray value, mean, standard deviation and 14 texture features proposed by [Haralick et al., 1973].

On the other hand, the model will use the information from initial partition for training a SOM in a supervised way. Then, FCM algorithm will be used to group prototypes; this

strategy tries to explode the topological information of SOM to forming a cluster represented by a subset of SOM prototypes. The fuzzy approach provided by FCM will allow estimating the proportions of each class in a pv-element. The output of the model will be presented as a partial volume estimation map (PVEM), but if necessary it may be transformed into a hard format using a maximum membership approach.

#### 4.1 Justification and Motivation

Because of the nature of PVE (spatial resolution and spatial sampling), the problem may be addressed as a pattern recognition task. Even, when there is a lot of research about brain MRI segmentation, most of it revolves around feature optimization, while few part of such study has been focused on reference data issues although it may help reduce the overlapping among classes and improving the segmentation results of the model [Abdelsamea et al., 2015, Ahmadvand and Daliri, 2015, Yazdani et al., 2016]. For instance, feature reduction through GA or principal component analysis (PCA) provides the most discriminative features to improve the segmentation result. Nevertheless, both of them analyze the feature vectors from pure and mixed IEs they may not avoid the bias added by pv-elements. Even though several approaches have been proposed to reduce the bias added by pv-elements, it remains as knowledge gap that requires attention because it is an ill-posed problem.

Brain tissue understanding and characterization are some of the most important goals for computer imaging science in medical domains [Madabhushi and Lee, 2016]. Since most of the interest in the brain focuses on analyzing it when it is working, in-vivo studies are highly desirable. MRI is one of the principal images modalities selected by scientists to perform studies concerning the brain structure, because of its advantages with regard to other modalities (non-ionizing radiation and minimum dependence of tracers). However, a key point in the studies of the brain depends on the correct identification of ROIs.

Providing solutions for the problem of correct identification of ROIs on brain MRIs, by incorporating a pre-selection stage to impose constraints for the reduction in the overlapping among the features of the ROIs, may produce new knowledge or solutions that improve the quality of the classification-segmentation and unveil information from the brain structure. The main goal of this research is to perform a pre-selection stage that identifies and selects IEs affected the least by PVE for the representation of CSF, GM and WM classes. As well as the development of a classifier that uses the pre-selected information with the purpose of determining the boundaries that represent each class, estimating the proportions of each class in a pv-element, and assigning this kind of elements to a single class.

#### 4.2 Research questions

The research questions that guide this research are:

- How can a non-overlapping partition be achieved between homogeneous regions and regions composed of pv-elements in T1-weighted scans of the brain?

- How can be used the information from homogeneous regions for estimating the tissue proportions in each pv-element?
- What are the implications of making a hard classification of the pv-elements through a partial estimation of these in T1-weighted scans of the brain?

### 4.3 Hypothesis

The hypothesis driving this research is:

*A model based on seeded region growing, self-organized maps and fuzzy clustering may improve the classification of pv-elements in brain magnetic resonances, restricted to T-1 weighted, when an initial partition is established, in comparison with other methods addressing this kind of classification problem.*

### 4.4 Aim

The aim of this research is to develop and validate a hybrid computational model to overcome the challenges introduced by PVE on brain MRIs and to achieve a precise classification of the brain tissues.

#### Specific Objectives

- To propose an extension of a segmentation algorithm based in SRG, so that it can separate pure IEs from pv-elements on a single channel brain MRI.
- To develop strategies to incorporate fuzzy clustering among SOM's elements to improve the pv-elements classification in T1-weighted brain MRI.

### 4.5 Expected contributions

The proposed research work aims at the following contributions:

- An extension of a segmentation algorithm based on SRG to identify and separate homogeneous regions from regions formed by pv-elements. Furthermore, the extension of the SRG algorithm will automatically seed and incorporate a reallocation process for reassigning IEs that were wrongly segmented.
- A model based on SOM-FCM to address PVS on brain MRI.

## 5 Methodology

To reach the objectives and answer the research questions raised in this Ph.D. research, the following methodology is proposed:

1. Application domain characterization.- In this phase, the required datasets will be gathered and characterized. The characterization step determines the necessary parameters that images must have to achieve the goal.
  - Data selection
    - BrainWeb from the McConnell Brain Imaging Centre [[Cocosco et al., 1997](#)]. A MRI simulator creates synthetic images of the brain by using anatomical models.
    - Internet Brain Segmentation Repository (IBSR) from the Massachusetts General Hospital. IBSR contains real images from patients, including ground truth data for each of them [[IBSR, 2010](#)].
  - Removal of non-brain tissue.- There are some non-brain tissues such as fat, skull, dura and marrow whose intensities might overlap with the intensities of brain tissues. These tissues are not of interest for the study of brain tissues; therefore they are removed using BrainSuite [[Shattuck et al., 2001](#)].
2. To develop an extension of a segmentation algorithm.- with the purpose of separating homogeneous regions from regions formed of pv-elements, an extension of SRG algorithm proposed by [[Adams and Bischof, 1994](#)] will be developed. The algorithm receives as input a T1-weighted scan, while it provides as output four sets; three of them composed of pure IEs and one formed by pv-elements. Key points in the SRG extension are:
  - To develop a method for seed selection. A seed must satisfy three criteria proposed by [[Shih and Cheng, 2005](#)]:
    - (a) High similarity to its neighbors
    - (b) At least one seed must be placed in each ROI
    - (c) Seeds for different ROIs must be disconnected
  - Penalize IEs that do not meet the homogeneity test. Penalization has the intention of excluding extreme values in the growing process of seeds, which may lead to a failure in algorithm goal.
  - To propose a reallocation process that reassigning IEs that were penalized or assigned into a wrong set [[Ahmadvand and Daliri, 2015](#)].

The Area-Fit-Index (AFI) [[Neubert et al., 2008](#)] will be used for the assessment of results, which was used in [[Morales et al., 2014](#)] to quantify the difference of areas between the reference object and the segmented object. It is defined by equation (16)

$$AFI = \frac{Area_{ref} - Area_{seg}}{Area_{ref}} \quad (16)$$

3. Pattern representation.- by using the initial partition from the proposed extension of SRG, a set of transformations on the IEs will be performed. Each IE will be represented by a feature vector composed of first order statistics and textural features in similar way as in the work of [Ortiz et al., 2013a].
4. Partial estimation.- a hybrid model based on SOM-FCM will implemented to address the partial volume estimation of each pv-element on a brain MRI. The next points must be covered to achieve the goal:
  - Initialization of prototypes.- following the assumption that a good initial map, refined by SOM training may provide a better representation of the feature space, we initialize SOM prototypes using the scheme proposed by Su [Su et al., 1999] to work with the three patterns with the largest inter-pattern distance (i.e., the CSF, GM and WM classes).
  - Shortcut winner strategy.- under the premise that the BMU of a pattern is in the neighborhood of the BMU for the previous epoch [Engelbrecht, 2007]. This step has the purpose of improving the convergence speed of the model.
  - Clustering SOM prototypes.- grouping similar prototypes into a single cluster that represents the same class may act as BMU for a subset of the data manifolds. Furthermore, it is necessary to estimate membership degree of a pv-element to a cluster. Hence, the FCM algorithm [Bezdek et al., 1981] is incorporated to SOM for achieving both tasks, grouping prototypes and calculating memberships degrees. FCM for SOM can be formulated as follows:

$$J_m = \sum_{i=1}^N \sum_{j=1}^C \mu_{ij}^m \|w_i - c_j\|^2 \quad (17)$$

where,  $N$  is the number of data samples,  $C$  is the number of clusters (CSF, GM, and WM),  $w_i$  is a prototype of the SOM,  $\mu_{ij}^m$  is the membership function defined as:

$$\mu_{ij} = \sum_{k=1}^C \left\| \frac{w_i - c_j}{w_i - c_k} \right\|^{-\frac{2}{m-1}} \quad (18)$$

where  $c_j$  is the center of the  $j$ th cluster. However, since each SOM's element is a cluster optimized there is no need to recalculate centroids for FCM. Therefore, each IE can be assigned to a different cluster with its corresponding membership degree. Finally, the result of the hybrid model will be a PVEM of the brain tissues on a MRI. The CFCM described in equation (14) will be used to evaluate the results of partial estimation.

5. Transform a PVEM into a hard representation.- This with the purpose of using the computational model on real brain MRI where the ground truth consists of non-overlapped sets. Initially, we intend to use maximum membership criterion to defuzzify PVEM.

6. Implementation and Validation.- The proposed model will be implemented, followed by a validation process through experimental design.

- Internal validity.- to compare the segmentation result of the method with the ground truth. The JAC index [Taha and Hanbury, 2015] will be used as evaluation metric.
- Concurrent validity.- to compare the segmentation result of the method with the work of other authors. The comparison will be made with four works:
  - (a) [Yazdani et al., 2016], this work is based on an extension of SRG.
  - (b) [Zhang et al., 2017], this work is based on an extension of FCM.
  - (c) [Ortiz et al., 2013b], this work is based on SOM.

## 5.1 Experiments

This section describes the experiments that will be performed to validate the hybrid computational model.

### Experiment 1 (E1)

**SRG algorithm extension evaluation.**- the proposed SRG extension will separate pure IEs from pv-elements. The ROIs correspond to three different tissue classes: CSF, GM and WM. Non-brain tissues will be removed by using BrainSuite [Shattuck et al., 2001].

**Aim:** to test the extension of the SRG algorithm for the localization and segmentation of pure IEs from pv-elements on a single channel brain MRI by analyzing their gray level distribution.

**H1:** it is possible to separate pure IEs from pv-elements on a brain MRI by analyzing their gray level distribution.

**Experimental design:**

*Experimental unit:* single channel brain MRI.

*Independent variable:* proposed SRG extension algorithm.

*Dependent variable:* achieved segmentation.

*Potential sources of bias:* model implementation.

*Evaluation:* experiment will be evaluated at two levels of validity, internal and criterion.

### Experiment 2 (E2)

**Evaluation of the proposed hybrid computational model.**- the proposed hybrid model will address PVS on brain MRIs.

**Aim:** testing the model performance to classify pv-elements on brain MRI.

**H2:** the use of pre-selected information combined with a hybrid computational model based on SOM-FCM may lead to better results on PVS issues on brain MRI.

**Experimental design:**

*Experimental unit:* single channel brain MRI.

*Independent variables:* pre-selected information from E1 and the proposed hybrid computational model.

*Dependent variable:* achieved classification.

*Potential sources of bias:* model implementation.

*Evaluation:* experiment will be evaluated at two levels of validity, internal and criterion.

## 5.2 Work plan

The schedule in Figure 11 shows the proposed activities for the development of this research.

Activity		2016	2017			2018			2019			2020	
		Sept-Dec	Jan-Apr	May-Aug									
1	Literature review												
2	Research goal definition												
3	Application domain characterization												
4	Design of hybrid computational model												
	4.1 Development of the SRG extension												
	4.2 Feature representation												
	4.3 Design of the SOM-FCM model												
5	Experiments				Sept		Jun		Jan-Feb				
6	Result evaluation				Oct		Jul-Aug	Sept	Mar-Apr	May			
7	Research progress review				Dec			Dec			Dec		
8	Writing of papers				Nov-Dec			Oct-Nov		Jun-Jul	Oct-Nov		
9	Writing of the thesis									Aug			
10	Thesis defense												

Figure 11. Work Plan.

## 6 Preliminary results

This section describes the results obtained during the development of an extension of the SRG algorithm. Synthetic images were used to test the performance of the algorithm.

### 6.1 Synthetic images of the brain

BrainWeb provides 20 anatomical models of 20 healthy brains. Each set contains the masks (sets of labeled image elements) of 9 tissues (cerebrospinal fluid, gray matter, white

matter, fat, muscle, muscle/skin, skull, blood vessels, connective (region around fat), dura matter and bone marrow). Each model is used to create a synthetic brain MRI. The model is blurred by a Gaussian mask ( $9 \times 9$  size) to simulate PVE. Furthermore, 3%, 5%, 7% and 9% of Rician distributed random noise was added to simulate the noise present in a real MRI as in the work of [Tohka, 2013] (see Figure 12).

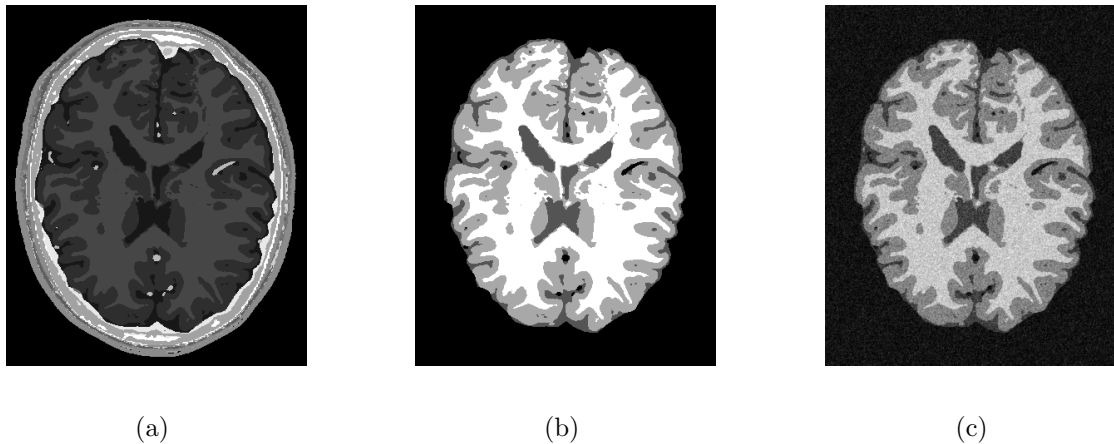


**Figure 12. Synthetic image; (a) masks of the anatomy of the brain, (b) skull stripped, and (c) synthetic images of brain tissues (CSF, GM and WM) corrupted by 7% of Rician noise.**

## 6.2 SRG extension

The extension of SRG is divided in three steps, seeded, growing and reallocation. The seeded process was performed by analyzing the histogram of the image. As it can be observed in Figure 13, the histogram presents three main peaks. The first peak corresponds to the CSF, the second to GM and the third to WM. The seeds for each class are selected with  $S = k_a \leq I(P_c) \leq k_b$ , where  $S$  is the set of seeds for each ROI,  $I$  is the observed image intensity,  $P_c$  is the peak value of each class, and  $k_a$  and  $k_b$  are thresholds. Then, the quality of each seed is evaluated with a factor  $q = \mu_{s_i} / \sigma_{s_i}$ , where  $\mu_{s_i}$  is the mean and  $\sigma_{s_i}$  is the standard deviation, both statistics are calculated over a window of  $3 \times 3$ . Those seeds with a  $q \geq \tau$ , are selected as *good seeds* and used for the growing process,  $\tau$  is a threshold value selected.

The growing process incorporates new elements into a region if they satisfy a homogeneity criterion. In this research, a measure based on the mean and standard deviation at a local and global level was chosen. Algorithm 1 describes the growing process. Each IE is considered as a candidate for being added to a ROI. Line 3 describes the first test for a candidate, if the candidate fails the test it is penalized and excluded from the growing process. We define two kinds of homogeneity measures, local and global. A global homogeneity test (line 4) is

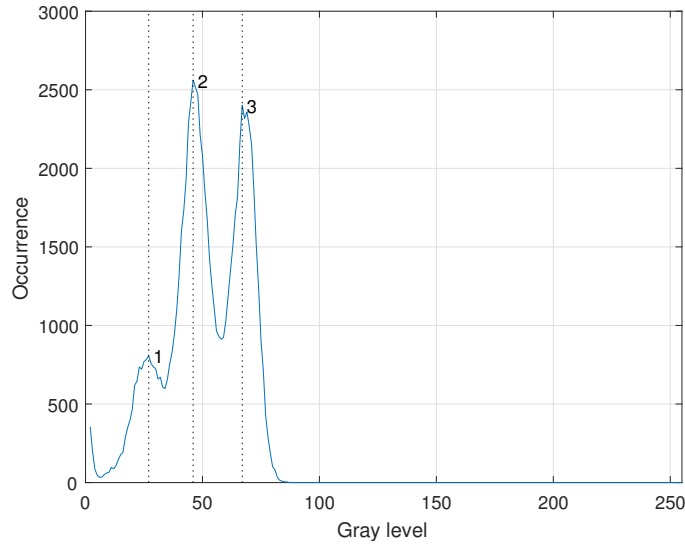


**Figure 13. Histogram of one synthetic brain MRI corrupted with 7% of Rician noise.**

used to evaluate the first neighborhood of the  $i$ th seed;  $\mu_g$  and  $\sigma_g$  are the mean and standard deviation gray value of the seed set that represent a ROI. Once the  $i$ -th seed has grown for the first time, the added elements are used to define a local homogeneity test (line 5) based on similar metrics as in line 4. Nevertheless,  $\mu_l$  and  $\sigma_l$  are updated every time that new candidates are added. Finally,  $R_c$  contains the candidates corresponding to classes CSF, GM and WM.  $P_c$  contains all the penalized candidates. Later, penalized candidates will have a second chance to be added to a class by a reallocation process described by Eq. 19.

---

**Algorithm 1: Growing**

---

**Data:** MRI of the brain

**Result:** Partition  $R_c$

```

1 foreach seed do
2   foreach candidate do
3     if the candidate has not been penalized or added to other ROI then
4       if the candidate is near to the seed &  $|I(\text{candidate}) - \mu_g| \leq \alpha\sigma_g$  then
5          $R_c \leftarrow \text{candidate};$ 
6       else if  $|I(\text{candidate}) - \mu_l| \leq \alpha\sigma_l$  then
7          $R_c \leftarrow \text{candidate};$ 
8       else  $P_c \leftarrow \text{candidate};$ 
9     end
10  end

```

---

$$Reallocation(P_c) = \begin{cases} 1 & \mu_{R_c} - 3\sigma_{R_c} \leq I(P_c) \leq \mu_{R_c} + 3\sigma_{R_c} \\ 0 & otherwise \end{cases} \quad (19)$$

where  $\mu_{R_c}$  is the mean gray value and  $\sigma_{R_c}$  the standard deviation of class  $R_c$ . This metric has the purpose of excluding extreme values [DeGroot et al., 1986]. The recovered candidates are reallocated to the corresponding class. Figure 14 depicts an example of segmentation obtained by the proposed extension of SRG.

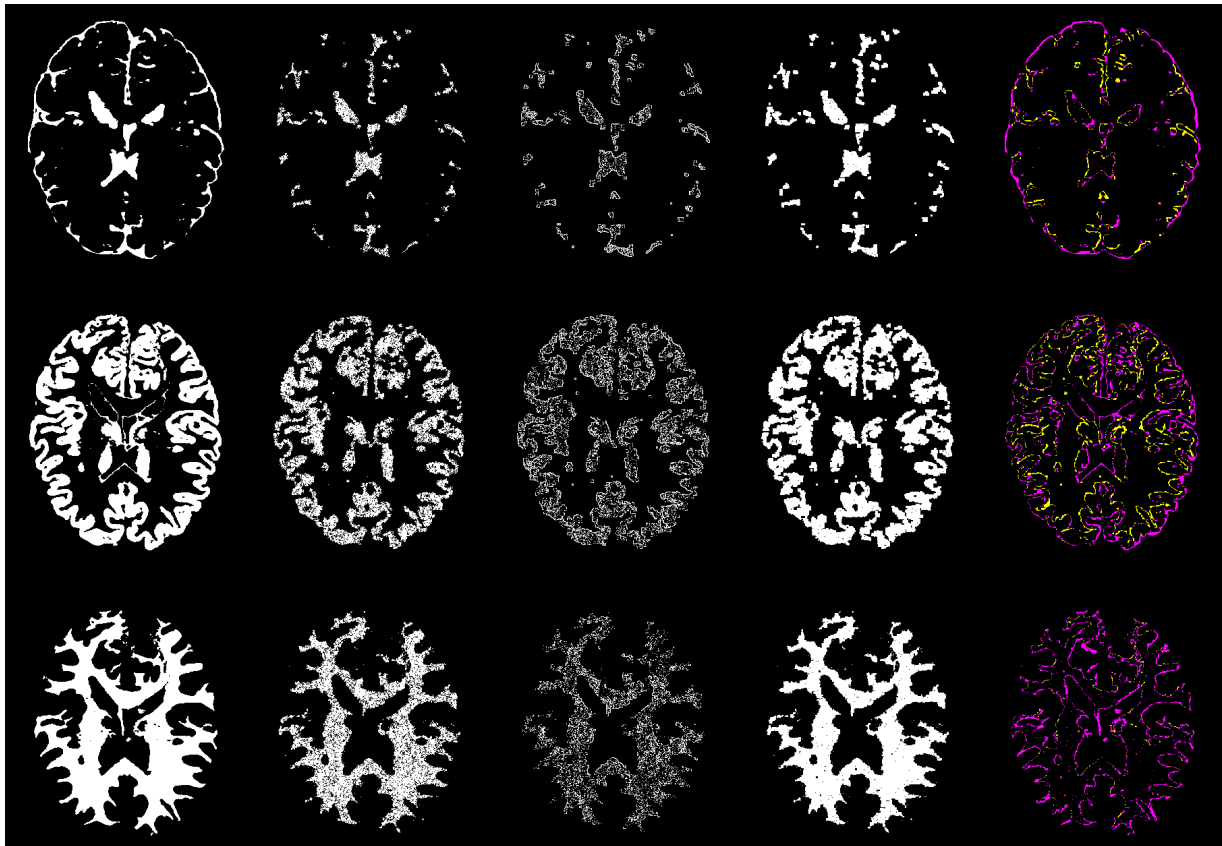


Figure 14. Result of the extension of SRG. The process for CSF is depicted in the first row, for GM in the second row and for WM in the third row. The first column shows the ground truth. The second column shows growing process. The third column shows penalized elements. The fourth column shows the final result of SRG. The fifth column shows the errors, **yellow** for false positive and **pink** for false negative.

### 6.3 Discussion

The proposed extension of SRG obtains better segmentation results than the original SRG. This result is in part to the seeding process, while the original SRG requires manual process (which is complicated in certain areas where the structures are blurred) the proposed extension can put seeds in zones where an operator may have problems with placing seeds. Furthermore, due to the noise, the growing process of the original SRG stops prematurely, while the proposed extension can analyze and add a greater amount of elements. This because to the local analysis and the reallocation process incorporated in the proposed extension of SRG.

As shown Table 3, the best results were obtained for WM when the images are affected by noise levels above 5%. This because the gray distribution of WM presents lower overlapping concerning to CSF and GM. JAC index for GM is lower than WM because GM has the biggest perimeter, which means it has a lot of IEs affected by PVE. On the other hand, the proposed extension of SRG has problems identifying IEs of CSF because many of them are in zones where CSF is thin, and PVE affects almost at all IEs. All those factors cause the JAC index for CSF is the lowest of the three, but the result obtained by the proposed extension of SRG for CSF and GM are better than the obtained by the original SRG. However, it is necessary to improve growing processes. The reallocation process, even when its operating principle is quite simple, it proved to be useful to recover IEs that were wrongly penalized. However, it is necessary to improve it and extend it to operate on IEs that were wrongly assigned to CSF, GM or WM classes.

**Table 3. Performance chart of the original SRG and the proposed extension with the Brain-Web [Cocosco et al., 1997] data set.  $\rho$  stands for Jaccard index,  $\alpha$  stands for Sensitivity and  $\beta$  stands for Specificity.**

Method	Noise %	CSF			GM			WM		
		$\rho$	$\alpha$	$\beta$	$\rho$	$\alpha$	$\beta$	$\rho$	$\alpha$	$\beta$
SRG	3%	0.318	0.694	0.787	0.701	0.859	0.902	0.820	0.821	0.999
	5%	0.105	0.9903	0.212	0.436	0.999	0.632	0.849	0.878	0.991
	7%	0.114	0.990	0.2663	0.430	0.999	0.6326	0.4212	1.000	0.628
	9%	0.106	0.992	0.212	0.430	0.999	0.632	0.420	1.000	0.628
Proposed	3%	0.515	0.525	0.998	0.742	0.760	0.993	0.797	0.798	0.999
	5%	0.569	0.603	0.995	0.776	0.845	0.975	0.827	0.834	0.997
	7%	0.577	0.674	0.985	0.730	0.854	0.952	0.792	0.805	0.995
	9%	0.472	0.741	0.939	0.580	0.713	0.935	0.750	0.764	0.994

## 7 Conclusion

This document presents the Ph.D. research of the project in development. The research is focused on proposing a hybrid computational model to address PVS on brain MRIs. The goal of the model is to accurately segment those IEs that correspond to CSF, GM and WM tissue classes.

As a preliminary result, an extension of the SDR algorithm has been developed, whose objective is performing a pre-selection stage to separate pure IEs from pv-elements. The SDR algorithm incorporates local and global information for seeding and growing. Furthermore, in contrast with other variants of SRG, the proposed algorithm includes a reallocation step for the detection of IEs that were misclassified because they did not meet the homogeneity criterion. The proposed SRG extension achieved favorable results, but it still needs to be refined in order to correct deficiencies and it needs to be tested with real MRIs. Regarding the SOM-FCM classifier, as of now, the related works about SOM and FCM have been reviewed, and some tests of the algorithms have been implemented to explore and understand the operation of both methods. However, the steps for the SOM-FCM classifier described in the methodology have not been implemented yet.

## References

- [Abdelsamea et al., 2015] Abdelsamea, M. M., Gnecco, G., and Gaber, M. M. (2015). An efficient self-organizing active contour model for image segmentation. *Neurocomputing*, 149:820–835.
- [Adams and Bischof, 1994] Adams, R. and Bischof, L. (1994). Seeded region growing. *IEEE Transactions on pattern analysis and machine intelligence*, 16(6):641–647.
- [Ahmadvand and Daliri, 2015] Ahmadvand, A. and Daliri, M. R. (2015). Improving the runtime of mrf based method for mri brain segmentation. *Applied Mathematics and Computation*, 256:808–818.
- [Anitha and Murugavalli, 2016] Anitha, V. and Murugavalli, S. (2016). Brain tumour classification using two-tier classifier with adaptive segmentation technique. *IET Computer Vision*, 10(1):9–17.
- [Bezdek et al., 1981] Bezdek, J. C., Coray, C., Gunderson, R., and Watson, J. (1981). Detection and characterization of cluster substructure I. Linear structure: Fuzzy C-lines. *SIAM Journal on Applied Mathematics*, 40(2):339–357.
- [Budayan et al., 2009] Budayan, C., Dikmen, I., and Birgonul, M. T. (2009). Comparing the performance of traditional cluster analysis, self-organizing maps and fuzzy c-means method for strategic grouping. *Expert Systems with Applications*, 36(9):11772–11781.
- [Buxton, 2009] Buxton, R. B. (2009). *Introduction to functional magnetic resonance imaging: principles and techniques*. Cambridge university press.
- [Cheng, 2002] Cheng, T. (2002). Fuzzy objects: their changes and uncertainties. *Photogrammetric Engineering and Remote Sensing*, 68(1):41–50.
- [Choi et al., 1991] Choi, H. S., Haynor, D. R., and Kim, Y. (1991). Partial volume tissue classification of multichannel magnetic resonance images: a mixel model. *IEEE Transactions on Medical Imaging*, 10(3):395–407.
- [Christiansen, 2016] Christiansen, B. A. (2016). Effect of micro-computed tomography voxel size and segmentation method on trabecular bone microstructure measures in mice. *Bone Reports*, 5:136–140.
- [Cocosco et al., 1997] Cocosco, C. A., Kollokian, V., Kwan, R. K.-S., Pike, G. B., and Evans, A. C. (1997). Brainweb: Online interface to a 3D MRI simulated brain database. In *NeuroImage*. Citeseer.
- [Crum et al., 2006] Crum, W. R., Camara, O., and Hill, D. L. (2006). Generalized overlap measures for evaluation and validation in medical image analysis. *IEEE transactions on medical imaging*, 25(11):1451–1461.

- [DeGroot et al., 1986] DeGroot, M. H. M. H. et al. (1986). *Probability and statistics*. Number 04; QA273, D4 1986.
- [Deserno, 2011] Deserno, T. M. (2011). Fundamentals of biomedical image processing. *Biomedical Image Processing*, pages 1–51.
- [Despotović et al., 2015] Despotović, I., Goossens, B., and Philips, W. (2015). MRI segmentation of the human brain: challenges, methods, and applications. *Computational and mathematical methods in medicine*, 2015.
- [Dogdas et al., 2005] Dogdas, B., Shattuck, D. W., and Leahy, R. M. (2005). Segmentation of skull and scalp in 3D human MRI using mathematical morphology. *Human brain mapping*, 26(4):273–285.
- [Douaud et al., 2007] Douaud, G., Smith, S., Jenkinson, M., Behrens, T., Johansen-Berg, H., Vickers, J., James, S., Voets, N., Watkins, K., Matthews, P. M., et al. (2007). Anatomically related grey and white matter abnormalities in adolescent-onset schizophrenia. *Brain*, 130(9):2375–2386.
- [El-Dahshan et al., 2014] El-Dahshan, E.-S. A., Mohsen, H. M., Revett, K., and Salem, A.-B. M. (2014). Computer-aided diagnosis of human brain tumor through MRI: A survey and a new algorithm. *Expert systems with Applications*, 41(11):5526–5545.
- [Engelbrecht, 2007] Engelbrecht, A. P. (2007). *Computational intelligence: an introduction*. John Wiley & Sons.
- [Fairchild, 2013] Fairchild, M. D. (2013). *Color appearance models*. John Wiley & Sons.
- [Fan et al., 2005] Fan, J., Zeng, G., Body, M., and Hacid, M.-S. (2005). Seeded region growing: an extensive and comparative study. *Pattern recognition letters*, 26(8):1139–1156.
- [Gong et al., 2013] Gong, M., Liang, Y., Shi, J., Ma, W., and Ma, J. (2013). Fuzzy c-means clustering with local information and kernel metric for image segmentation. *IEEE Transactions on Image Processing*, 22(2):573–584.
- [Gonzalez and Woods, 2007] Gonzalez, R. C. and Woods, R. E. (2007). *Image processing*. Prentices Hall.
- [Gruppen and Buvat, 2011] Gruppen, C. and Buvat, I. (2011). *Handbook of particle detection and imaging*. Springer Science & Business Media.
- [Gui et al., 2012] Gui, L., Lisowski, R., Faundez, T., Hüppi, P. S., Lazeyras, F., and Kocher, M. (2012). Morphology-driven automatic segmentation of MR images of the neonatal brain. *Medical image analysis*, 16(8):1565–1579.

- [Güler et al., 2009] Güler, İ., Demirhan, A., and Karakış, R. (2009). Interpretation of MR images using self-organizing maps and knowledge-based expert systems. *Digital Signal Processing*, 19(4):668–677.
- [Haralick et al., 1973] Haralick, R. M., Shanmugam, K., et al. (1973). Textural features for image classification. *IEEE Transactions on systems, man, and cybernetics*, 3(6):610–621.
- [Haris et al., 1998] Haris, K., Efstratiadis, S. N., Maglaveras, N., and Katsaggelos, A. K. (1998). Hybrid image segmentation using watersheds and fast region merging. *IEEE transactions on image processing : a publication of the IEEE Signal Processing Society*, 7 12:1684–99.
- [Haykin et al., 2009] Haykin, S. S., Haykin, S. S., Haykin, S. S., and Haykin, S. S. (2009). *Neural networks and learning machines*, volume 3. Pearson Upper Saddle River, NJ, USA:.
- [Helmy and El-Taweel, 2016] Helmy, A. K. and El-Taweel, G. S. (2016). Image segmentation scheme based on som-pcnn in frequency domain. *Applied Soft Computing*, 40:405–415.
- [Hu, 1962] Hu, M.-K. (1962). Visual pattern recognition by moment invariants. *IRE Transactions on information theory*, 8(2):179–187.
- [IBSR, 2010] IBSR (2010). Internet Brain Database Repository, Massachusetts General Hospital, Center for Morphometric Analysis.
- [Jain and Dubes, 1988] Jain, A. K. and Dubes, R. C. (1988). *Algorithms for clustering data*. Prentice-Hall, Inc.
- [Jain et al., 2000] Jain, A. K., Duin, R. P. W., and Mao, J. (2000). Statistical pattern recognition: A review. *IEEE Transactions on pattern analysis and machine intelligence*, 22(1):4–37.
- [Jain et al., 1999] Jain, A. K., Murty, M. N., and Flynn, P. J. (1999). Data clustering: a review. *ACM computing surveys (CSUR)*, 31(3):264–323.
- [Jansi and Subashini, 2014] Jansi, S. and Subashini, P. (2014). Modified FCM using genetic algorithm for segmentation of mri brain images. In *Computational Intelligence and Computing Research (ICCIC), 2014 IEEE International Conference on*, pages 1–5. IEEE.
- [Kang and Kim, 2014] Kang, M. and Kim, J.-M. (2014). Fuzzy c-means clustering with spatially weighted information for medical image segmentation. In *Computational Intelligence for Multimedia, Signal and Vision Processing (CIMSIVP), 2014 IEEE Symposium on*, pages 1–8. IEEE.
- [Kannan et al., 2012] Kannan, S., Ramathilagam, S., Devi, R., and Hines, E. (2012). Strong fuzzy c-means in medical image data analysis. *Journal of Systems and Software*, 85(11):2425–2438.

- [Kohonen, 2001] Kohonen, T. (2001). Self-organizing maps. *Springer*.
- [Kohonen, 2013] Kohonen, T. (2013). Essentials of the self-organizing map. *Neural Networks*, 37:52–65.
- [Lalwani and Ansari, 2012] Lalwani, S. and Ansari, U. (2012). A new approach for increase resolution of satellite image.
- [Li et al., 2015] Li, S., Yao, J., et al. (2015). *Spinal Imaging and Image Analysis*. Springer.
- [Li et al., 2003] Li, X., Eremina, D., Li, L., and Liang, Z. (2003). Partial volume segmentation of medical images. In *Nuclear Science Symposium Conference Record, 2003 IEEE*, volume 5, pages 3176–3180. IEEE.
- [Liao et al., 2008] Liao, L., Lin, T., and Li, B. (2008). MRI brain image segmentation and bias field correction based on fast spatially constrained kernel clustering approach. *Pattern Recognition Letters*, 29(10):1580–1588.
- [Lin et al., 2012] Lin, G.-C., Wang, W.-J., Kang, C.-C., and Wang, C.-M. (2012). Multi-spectral MR images segmentation based on fuzzy knowledge and modified seeded region growing. *Magnetic resonance imaging*, 30(2):230–246.
- [Liu and Guo, 2015] Liu, J. and Guo, L. (2015). A new brain mri image segmentation strategy based on k-means clustering and svm. In *Intelligent Human-Machine Systems and Cybernetics (IHMSC), 2015 7th International Conference on*, volume 2, pages 270–273. IEEE.
- [Liu et al., 2010] Liu, L., Wang, B., and Zhang, L. (2010). An approach based on self-organizing map and fuzzy membership for decomposition of mixed pixels in hyperspectral imagery. *Pattern Recognition Letters*, 31(11):1388–1395.
- [Lötjönen et al., 2010] Lötjönen, J. M., Wolz, R., Koikkalainen, J. R., Thurfjell, L., Walde-mar, G., Soininen, H., Rueckert, D., Initiative, A. D. N., et al. (2010). Fast and robust multi-atlas segmentation of brain magnetic resonance images. *Neuroimage*, 49(3):2352–2365.
- [Madabhushi and Lee, 2016] Madabhushi, A. and Lee, G. (2016). Image analysis and machine learning in digital pathology: challenges and opportunities.
- [Marroquin et al., 1987] Marroquin, J., Mitter, S., and Poggio, T. (1987). Probabilistic solution of ill-posed problems in computational vision. *Journal of the american statistical association*, 82(397):76–89.
- [Morales et al., 2014] Morales, J., Gonzalez, J. A., García, C. A. R., and Robles, L. A. (2014). Transition regions detection from satellite images based on evolutionary region growing segmentation. *Intell. Data Anal.*, 18:305–316.

- [Morales, 2014] Morales, J. C. (2014). *Obtención y clasificación de píxeles mezclados generados por regiones de transición en imágenes satelitales*. PhD thesis, INAOE.
- [Neubert et al., 2008] Neubert, M., Herold, H., and Meinel, G. (2008). Assessing image segmentation quality—concepts, methods and application. *Object-based image analysis*, pages 769–784.
- [Niessen et al., 1999] Niessen, W. J., Vincken, K. L., Weickert, J., Romeny, B. T. H., and Viergever, M. A. (1999). Multiscale segmentation of three-dimensional mr brain images. *International Journal of Computer Vision*, 31(2):185–202.
- [Noe and Gee, 2001] Noe, A. and Gee, J. C. (2001). Partial volume segmentation of cerebral MRI scans with mixture model clustering. In *IPMI*, pages 423–430. Springer.
- [Nordenskjöld, 2014] Nordenskjöld, R. (2014). *Analysis of Human Brain MRI: Contributions to Regional Volume Studies*. PhD thesis, Acta Universitatis Upsaliensis.
- [Ortiz et al., 2011] Ortiz, A., Górriz, J., Ramirez, J., and Salas-Gonzalez, D. (2011). MR brain image segmentation by growing hierarchical som and probability clustering. *Electronics Letters*, 47(10):585–586.
- [Ortiz et al., 2014] Ortiz, A., Górriz, J., Ramirez, J., and Salas-Gonzalez, D. (2014). Improving MR brain image segmentation using self-organising maps and entropy-gradient clustering. *Information Sciences*, 262:117–136.
- [Ortiz et al., 2013a] Ortiz, A., Górriz, J., Ramírez, J., Salas-Gonzalez, D., and Llamas-Elvira, J. M. (2013a). Two fully-unsupervised methods for MR brain image segmentation using SOM-based strategies. *Applied Soft Computing*, 13(5):2668–2682.
- [Ortiz et al., 2013b] Ortiz, A., Palacio, A. A., Górriz, J. M., Ramírez, J., and Salas-González, D. (2013b). Segmentation of brain MRI using SOM-FCM based method and 3D statistical descriptors. *Computational and mathematical methods in medicine*, 2013.
- [Péporté et al., 2011] Péporté, M., Ghita, D. E. I., Twomey, E., and Whelan, P. F. (2011). A hybrid approach to brain extraction from premature infant MRI. In *Scandinavian Conference on Image Analysis*, pages 719–730. Springer.
- [Pham et al., 2000] Pham, D. L., Xu, C., and Prince, J. L. (2000). Current methods in medical image segmentation. *Annual review of biomedical engineering*, 2(1):315–337.
- [Revol-Muller et al., 2013] Revol-Muller, C., Grenier, T., Rose, J.-L., Pacureanu, A., Peyrin, F., and Odet, C. (2013). Region growing: When simplicity meets theory—region growing revisited in feature space and variational framework. In *Computer Vision, Imaging and Computer Graphics. Theory and Application*, pages 426–444. Springer.

- [Ribes et al., 2014] Ribes, S., Didierlaurent, D., Decoster, N., Gonneau, E., Risser, L., Feillel, V., and Caselles, O. (2014). Automatic segmentation of breast mr images through a markov random field statistical model. *IEEE transactions on medical imaging*, 33(10):1986–1996.
- [Sainju et al., 2014] Sainju, S., Bui, F. M., and Wahid, K. A. (2014). Automated bleeding detection in capsule endoscopy videos using statistical features and region growing. *Journal of medical systems*, 38(4):25.
- [Santago and Gage, 1995] Santago, P. and Gage, H. D. (1995). Statistical models of partial volume effect. *IEEE Transactions on Image Processing*, 4(11):1531–1540.
- [Schiewe and Kinkeldey, 2009] Schiewe, J. and Kinkeldey, C. (2009). Development of an advanced uncertainty measure for classified remotely sensed scenes. *Proceedings for ISPRS WG II/2*, 3(4).
- [Sezgin et al., 2004] Sezgin, M. et al. (2004). Survey over image thresholding techniques and quantitative performance evaluation. *Journal of Electronic imaging*, 13(1):146–168.
- [Shattuck et al., 2001] Shattuck, D. W., Sandor-Leahy, S. R., Schaper, K. A., Rottenberg, D. A., and Leahy, R. M. (2001). Magnetic resonance image tissue classification using a partial volume model. *NeuroImage*, 13(5):856–876.
- [Shen et al., 2005] Shen, S., Sandham, W., Granat, M., and Sterr, A. (2005). MRI fuzzy segmentation of brain tissue using neighborhood attraction with neural-network optimization. *IEEE transactions on information technology in biomedicine*, 9(3):459–467.
- [Shih and Cheng, 2005] Shih, F. Y. and Cheng, S. (2005). Automatic seeded region growing for color image segmentation. *Image and vision computing*, 23(10):877–886.
- [Sikka et al., 2009] Sikka, K., Sinha, N., Singh, P. K., and Mishra, A. K. (2009). A fully automated algorithm under modified FCM framework for improved brain mr image segmentation. *Magnetic Resonance Imaging*, 27(7):994–1004.
- [Soret et al., 2007] Soret, M., Bacharach, S. L., and Buvat, I. (2007). Partial-volume effect in PET tumor imaging. *Journal of Nuclear Medicine*, 48(6):932–945.
- [Su et al., 1999] Su, M.-C., Liu, T.-K., and Chang, H.-T. (1999). An efficient initialization scheme for the self-organizing feature map algorithm. In *Neural Networks, 1999. IJCNN'99. International Joint Conference on*, volume 3, pages 1906–1910. IEEE.
- [Taha and Hanbury, 2015] Taha, A. A. and Hanbury, A. (2015). Metrics for evaluating 3D medical image segmentation: analysis, selection, and tool. *BMC medical imaging*, 15(1):29.

- [Thevenot et al., 2014] Thevenot, J., Chen, J., Finnilä, M., Nieminen, M., Lehenkari, P., Saarakkala, S., and Pietikäinen, M. (2014). Local binary patterns to evaluate trabecular bone structure from micro-CT data: application to studies of human osteoarthritis. In *European Conference on Computer Vision*, pages 63–79. Springer.
- [Tohka, 2013] Tohka, J. (2013). FAST-PVE: Extremely fast markov random field based brain MRI tissue classification. In *Scandinavian Conference on Image Analysis*, pages 266–276. Springer.
- [Van Leemput et al., 2003] Van Leemput, K., Maes, F., Vandermeulen, D., and Suetens, P. (2003). A unifying framework for partial volume segmentation of brain MR images. *IEEE Transactions on medical imaging*, 22(1):105–119.
- [Wang and Chen, 2012] Wang, C.-M. and Chen, R.-M. (2012). Automatic vector seeded region growing for Parenchyma classification in brain MRI. In *Advances in Brain Imaging*. InTech.
- [Wang et al., 2008] Wang, J., Kong, J., Lu, Y., Qi, M., and Zhang, B. (2008). A modified fcm algorithm for MRI brain image segmentation using both local and non-local spatial constraints. *Computerized medical imaging and graphics*, 32(8):685–698.
- [Xia et al., 2016] Xia, Y., Ji, Z., and Zhang, Y. (2016). Brain mri image segmentation based on learning local variational gaussian mixture models. *Neurocomputing*, 204:189–197.
- [Yazdani et al., 2016] Yazdani, S., Yusof, R., Karimian, A., Mitsukira, Y., and Hematian, A. (2016). Automatic region-based brain classification of MRI-T1 data. *PloS one*, 11(4):e0151326.
- [Zadeh, 1965] Zadeh, L. A. (1965). Fuzzy sets. *Information and control*, 8(3):338–353.
- [Zanaty and Asaad, 2013] Zanaty, E. and Asaad, A. (2013). Probabilistic region growing method for improving magnetic resonance image segmentation. *Connection Science*, 25(4):179–196.
- [Zhang et al., 2017] Zhang, X., Wang, G., Su, Q., Guo, Q., Zhang, C., and Chen, B. (2017). An improved fuzzy algorithm for image segmentation using peak detection, spatial information and reallocation. *Soft Computing*, 21(8):2165–2173.
- [Zhang et al., 2001] Zhang, Y., Brady, J. M., and Smith, S. M. (2001). An hmrf-em algorithm for partial volume segmentation of brain mri fmrib technical report tr01yz1. Technical report, Technical report, Oxford Centre for Functional Magnetic Resonance Imaging of the Brain.